

Growth of V_2O_3 thin films on a -plane (110) and c -plane (001) sapphire via pulsed-laser deposition

B.S. Allimi, S.P. Alpay,^{a)} and D. Goberman

*Materials Science and Engineering Program and Institute of Materials Science,
University of Connecticut, Storrs, Connecticut 06279*

T. Huang, J.I. Budnick, and D.M. Pease

*Department of Physics and Institute of Materials Science, University of Connecticut,
Storrs, Connecticut 06279*

A.I. Frenkel

Department of Physics, Yeshiva University, New York, New York 10016

(Received 23 April 2007; accepted 4 June 2007)

We report the direct deposition of epitaxial 215-nm-thick vanadium sesquioxide (V_2O_3) films on a - and c -plane sapphire substrates from powder-pressed V_2O_3 targets via pulsed-laser deposition (PLD) in an evacuated deposition chamber devoid of O_2 . The films were characterized using x-ray diffraction (XRD), x-ray photoemission spectroscopy (XPS), x-ray absorption fine structure (XAFS) spectroscopy, and atomic force microscopy (AFM). XPS measurements confirmed that the stoichiometry of the powder was conserved in the films. XRD patterns together with XAFS measurements proved that V_2O_3 was epitaxial on the a -sapphire substrate with epitaxial relation $(110)_{\text{film}} // (110)_{\text{substrate}}$, and the results are consistent with the epitaxy on the c -plane substrate as well. The room-temperature resistivities of V_2O_3 films on a - and c -plane substrates were 1.49×10^{-4} and $3.00 \times 10^{-5} \Omega \text{ m}$, respectively. The higher resistivities of the films compared to bulk V_2O_3 might be attributed to thermal stresses resulting from difference in thermal expansion coefficients (TECs) of the films and the substrates.

I. INTRODUCTION

Oxides of vanadium display a wide variety of structural and associated electronic phase transformations.¹ Of these, vanadium sesquioxide (V_2O_3) typifies this class of material system exhibiting a metal–insulator transition (MIT) as a function of temperature, pressure, and doping concentration.² At a transition temperature of 150 K, V_2O_3 transforms from a monoclinic antiferromagnetic insulator to a rhombohedral metallic state with a conductivity jump of ~ 7 orders of magnitude³ in the high-temperature phase. A broad second-order transition also occurs in the temperature range of ~ 450 – 500 K from metallic state to a semiconducting state. When doped with transition metals such as Cr or Ti, V_2O_3 undergoes additional transitions where the metallic phase can be stabilized with the addition of Ti_2O_3 and the insulating phase with the addition of Cr_2O_3 .² Due to these transitions, there is a significant interest in V_2O_3 , both in terms

of theoretical^{4–6} and experimental^{7–17} research. This interest is not only to explore the full potential of this material for technological applications but also to serve as a model for understanding the physics of the MIT itself.

Typically, crystal field theory is used to describe the phase transitions in V_2O_3 by relating the crystal and electronic band structures. Cation–anion–cation interactions and cation–cation interactions (in the basal plane and along the hexagonal c axis) provide a trigonal component to the octahedral crystal field which splits the t_{2g} orbital into a_{1g} along the c axis and $e_g(\pi)$ on the basal plane of the corundum structure.¹⁸ The metallic nature of the material above the critical temperature T_c results from overlapping of these bands. On the other hand, in the insulating state at low temperatures, the a_{1g} band is completely filled while the $e_g(\pi)$ band is completely empty with some energy separation between the two bands.¹⁸

To gain more understanding of this material and to explore its full potential for device applications such as thermal sensors, bolometers, and current limiters, various methods have been devised to synthesize high-quality V_2O_3 thin films. Deposition of thin films of this material

^{a)}Address all correspondence to this author.

e-mail: p.alpay@ims.uconn.edu

DOI: 10.1557/JMR.2007.0378

poses significant challenges because the range of processing parameters for stoichiometric V_2O_3 is relatively small due to the existence of many different oxidation states of vanadium. Some of the existing approaches to conquer these challenges include but are not limited to sol-gel processes, pyrolysis, reactive dc magnetron sputtering, and electron-beam evaporation.^{9–12,14} Recently, pulsed-laser deposition (PLD) of V_2O_3 using sintered V_2O_5 targets to study the effect of strain on the material¹⁶ has also been reported. This same approach was used by another group using sintered V_2O_3 targets obtained from reduction of V_2O_5 in an H_2 atmosphere to study the effect of epitaxial strains.¹⁵

In this study, we have developed a straightforward method of PLD of V_2O_3 films using a powder-pressed pure V_2O_3 target in an evacuated deposition chamber—no oxygen pressure was introduced in the chamber to avoid oxidation of V_2O_3 to V_2O_5 . The target was prepared directly from commercially pure V_2O_3 powder, pressed into pellets without any additives or sintering procedure. This is a new approach of deposition that employs only green powder compacts without the use of sintering or subsequent heat-treatment processes that may ruin the stoichiometry of the target. Compared to other methods reported in the literature, this route appears to be relatively simple and straightforward without having to go through the reduction of V_2O_5 or other intervening processes. We show that high-quality epitaxial V_2O_3 thin films can be fabricated directly from V_2O_3 targets by limiting the oxygen content during growth.

II. FILM DEPOSITION AND CHARACTERIZATION

We fabricated PLD targets from commercial V_2O_3 powders (99.99% pure; Sigma-Aldrich, Inc., St. Louis, MO). About 1.54 g of this powder, without the addition of binder or other additives, was pressed into disk pellet of diameter 19 mm and ~1.5 mm thick using a mechanical pressing machine. A load pressure of ~15,000 pounds was applied to obtain a target dense enough for the ablation process. The pressed target was not sintered to avoid any possibility of the target composition being altered or compromised due to oxidation.

From this target, V_2O_3 films of thicknesses of ~215 nm were deposited by PLD. A KrF excimer laser (wavelength = 248 nm, pulse length = 20 ns) with a fluence of ~2.8 J/cm² and repetition rate of 6 Hz, corresponding to a growth rate of ~0.12 nm/s was focused on the V_2O_3 target rotating at 35 rpm. The deposition was performed on *a*-plane (110) and *c*-plane (001) Al_2O_3 substrates. The choice of the substrates was due to their similar crystal structure (corundum) to the film, which tends to promote epitaxial growth. We carefully cleaned the substrates using a series of procedures including 10–15 min of ultra-

sonic cleaning in acetone and ethanol to obtain substrates free of surface contamination. The substrates were then glued to the substrate holder with silver paste to ensure good thermal contact. The substrates were heated to 750 °C at a rate of 10 °C/min in a deposition chamber which had been evacuated to a base pressure of 1.7×10^{-6} Torr prior to the heating process. The deposition proceeded in the evacuated chamber without influx of O_2 , as V_2O_3 appears to be unstable under oxygen atmosphere. After deposition, the samples were slowly cooled to room temperature at a rate of 2 °C/min.

The structural, crystallographic, and surface properties of the films were examined by a variety of techniques. These include x-ray diffraction (XRD) using a Bruker (Madison, WI) D5005 four-circle diffractometer with $Cu K_\alpha$ radiation, x-ray absorption fine structure (XAFS) spectroscopy at the X-18 B line of the National Synchrotron Light Source (NSLS; Brookhaven National Laboratory, Brookhaven, NY), and atomic force microscopy (AFM) with an MFP-3D stand-alone AFM (Asylum Research, Santa Barbara, CA). We determined the thickness of the film by imaging the cross section of the sample using scanning electron microscopy (SEM) with a JSM-6335F field-emission SEM (JEOL, Tokyo, Japan). X-ray photoelectron spectroscopy (XPS) was used for chemical analysis of the film. Electrical properties of the films at room temperature were determined using a Lucas Labs 302 four-point probe with a Keithley 2400 digital SourceMeter (Keithley Instruments, Inc., Cleveland, Ohio).

III. RESULTS AND DISCUSSION

Figure 1 shows the diffraction pattern of the V_2O_3 target with all the peaks consistent with those of a typical bulk V_2O_3 powder sample (ICDD 34-0187), while Fig. 2

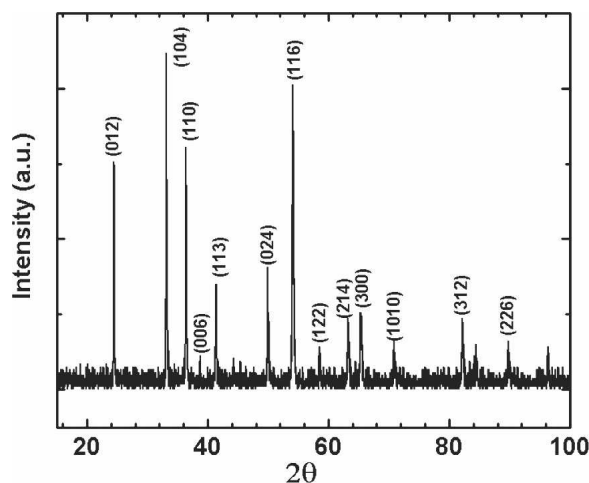


FIG. 1. XRD pattern of pressed PLD V_2O_3 target.

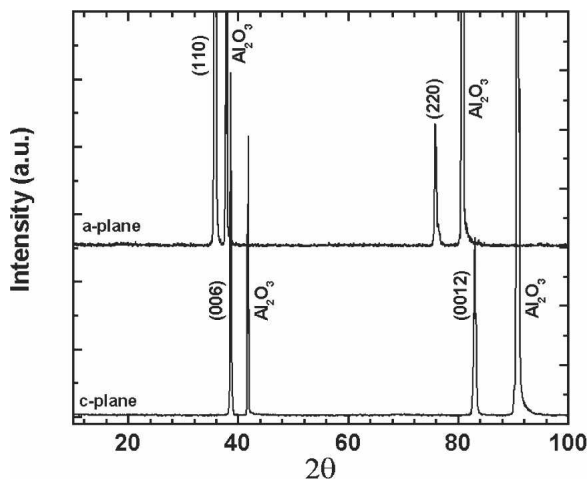


FIG. 2. XRD patterns of V_2O_3 films on *a*- and *c*-plane Al_2O_3 .

shows the diffraction patterns of the films on *a*- and *c*-plane sapphire substrates. The diffraction patterns of the films show that the films are highly oriented with the substrates, as only (00*l*)- and (*h**h*0)-type reflections in the θ - 2θ scan were present in the films on *c*- and *a*-plane sapphire substrates, respectively. We determined the interplanar spacings of the films normal to the surface by using the result of the substrates as calibration standards, and these results will be discussed in connection with the electrical resistivity measurements.

We also performed XAFS spectroscopy on these samples. Vanadium K-edge data were obtained at the X-18 B line of the NSLS, using silicon (111) crystals. The fluorescence method was used. For the *a*-plane substrate, by working with the incident beam direction perpendicular to the sapphire (110) plane, we rotated the sample so that we varied the sapphire *c*-axis angle relative to the horizontal direction, which is parallel to the synchrotron electric vector, *E*. We obtained vanadium edges that agreed with V_2O_3 absorption edges as shown in Fig. 3. Two peaks, A and B, are quite sensitive to the angle between the lattice parameter *c* and *E*.¹⁹ When peak A is at its maximum, *E* is applied along *c*; and when B is maximum, *E* is perpendicular to *c*. We find the angular dependence of these peaks corresponding exactly to an epitaxial alignment of the V_2O_3 with the sapphire (110) plane substrate. Were the film to be a fiber texture, and not epitaxial, we would have not observed these systematics. For the *c*-axis cut substrate, we observed for all rotations a pattern consistent with *E* perpendicular to *c*. This result for the *c*-plane substrate, does not prove, but is consistent with, epitaxy. Considering the smaller misfit on *c*-plane substrates, in addition to the x-ray diffraction data, we expect that films on *c*-plane substrate should grow epitaxially although XAFS cannot conclusively verify this.

Surface morphologies of the films were characterized

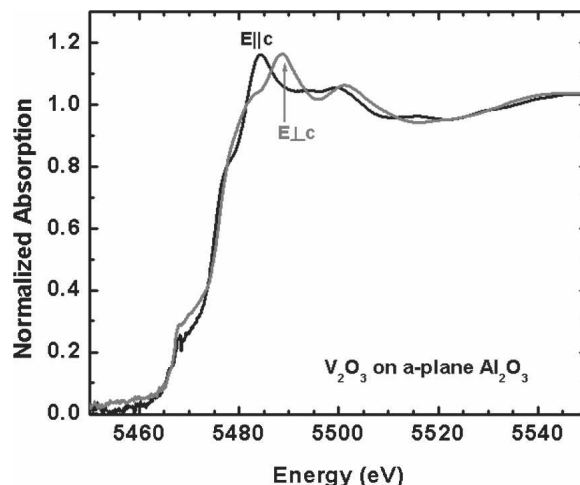


FIG. 3. XAFS spectra of V_2O_3 film on *a*-plane Al_2O_3 substrate. Peak positions and magnitudes shown for different angles between x-ray polarization and the *c*-axis of the substrate are identical to those measured in the oriented single-crystal V_2O_3 .³⁰

using AFM with a scan rate of 1 Hz and image resolution of 256×256 pixels. Figure 4(a) shows an AFM image of the surface topography of the V_2O_3 film on (001)-plane Al_2O_3 , revealing an extremely smooth surface. The surface roughness of the film is 0.445 nm. This may indicate that the growth of these films is via a layer-by-layer (Frank-van der Merwe) mode on the *c*-plane substrate. However, it is more likely that the growth mode is a mixed mode where the film may grow coherently until 60 nm thickness before forming misfit dislocations. This critical thickness follows from the thermodynamic analysis of Mathews and Blakeslee (MB),²⁰ with lattice parameters and thermal-expansion coefficients given in Tables I and II.

On the *a*-plane substrate [Fig. 4(b)], the surface roughness of the film is 3.4 nm. The relatively rougher surface suggests that the growth may have occurred via coalescence of islands [three-dimensional (3D) Volmer-Weber mode], where edge-type misfit dislocations are usually introduced at the periphery of the island to minimize the strain in the film.²¹ We note that this process also generates threading dislocations with a dislocation line vector that is not in the plane of film growth. The mismatch between the film and the substrate is relatively larger for growth on *a*-plane substrates and is anisotropic as well, as will be discussed in the subsequent sections. Thus, the MB critical thickness is between 5 and 7 nm along in-plane directions. The films in this case may have grown by the island mode as shown in Fig. 4(b). Although the surface roughness on *a*-plane substrate is relatively small, the AFM results suggest that the growth mechanism might be different from films on *c*-plane sapphire [Fig. 4(a)]. The difference in surface topography of these films, despite identical deposition conditions,

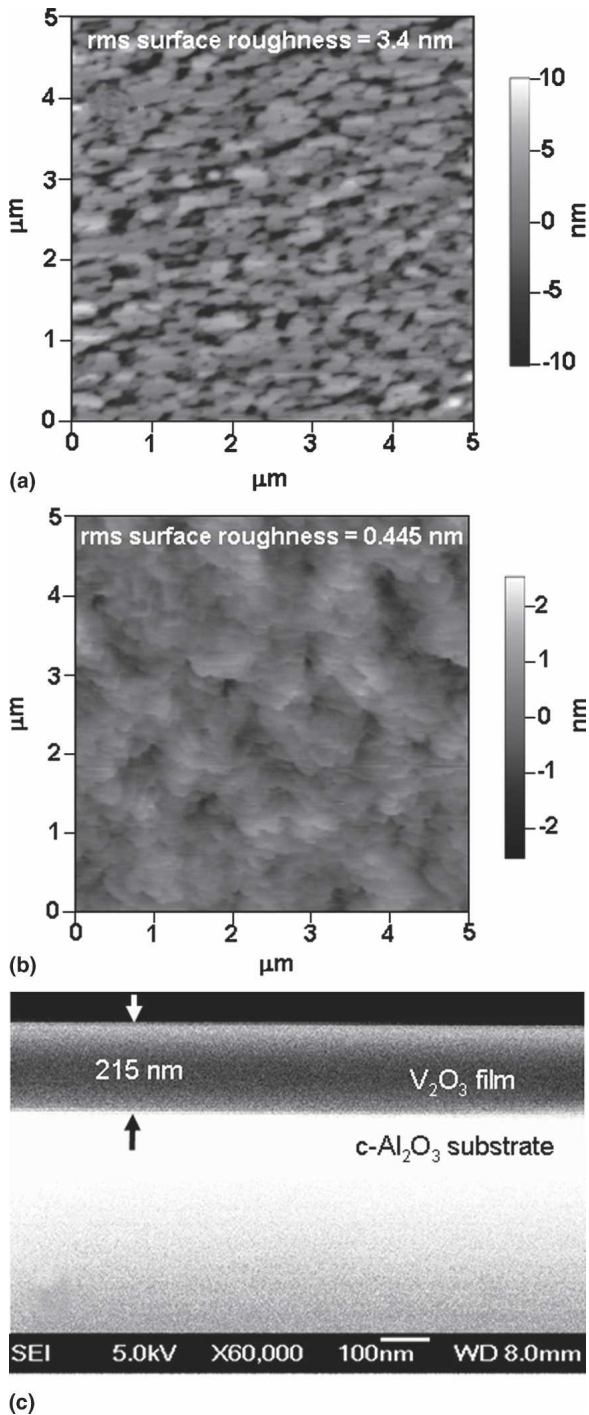


FIG. 4. AFM image of V₂O₃ films on (a) *c*-plane Al₂O₃, (b) *a*-plane Al₂O₃, and (c) SEM image of cross section of V₂O₃ film on *c*-plane sapphire substrate showing the 215-nm thickness of the film.

might be attributed to difference in the lattice mismatch between the films and their respective substrates (Table I).

We determined the thickness of the films by imaging the cross section of the samples using a JEOL JSM-6335F field-emission SEM. A 5-kV electron beam at 8-mm working distance was focused on the fractured

TABLE I. Theoretical in-plane lattice misfits and in-plane thermal strains of V₂O₃ film on sapphire substrate.^{2,26,27}

	Lattice parameter (nm)		ϵ_1, ϵ_2 (%)	α ($\times 10^{-5} \text{ }^\circ\text{C}^{-1}$)		$\epsilon_1^{th}, \epsilon_2^{th}$ (%)
	V ₂ O ₃	Al ₂ O ₃		V ₂ O ₃	Al ₂ O ₃	
a	0.4958	0.4758	-4.1	3.19	0.50	1.95
c	1.3958	1.2992	-7.4	-1.15	0.66	-1.32

TABLE II. Measured *d*-spacing of V₂O₃ films on *c*- and *a*-plane sapphire substrates compared to bulk value to compute out-of-plane misfits (experimental value is compared to theoretical value).

V ₂ O ₃ films on sapphire substrates	<i>d</i> -spacing (nm)		ϵ_3 (exp) (%)	ϵ_3 (%)	ϵ_3^{th} (%)
	Film	Bulk			
(001)	1.3949	1.4014	-0.464	3.6	-1.7
(110)	0.2505	0.2477	1.134	5.1	-0.3

edge section of the sample, and the image was captured using the secondary electron detector. In Fig. 4(c) we show a micrograph of the (001) V₂O₃ film on a (001) sapphire substrate. The thickness of the film is 215 nm, corresponding to a growth rate of 0.12 nm/s at 750 °C. Similar micrographs were obtained for films on *a*-plane sapphire (not included). Further SEM analysis showed that the thickness of the films remains constant across the width of the samples.

XPS was used to investigate the compositions of the films. In the XPS process, x-rays are used to excite core electrons from their initial energy levels. Those electrons that are within ~10 nm of the surface of a material may be ejected into the vacuum system. The kinetic energy of these electrons, or “photoelectrons,” is measured using an electron spectrometer. The difference between the excitation energy (in this case, Al K_α radiation) and the measured kinetic energy represents the energy required to move an electron from its initial level to the vacuum level in a particular material and is called the binding energy. This binding energy will change as the bonding state of the parent atom changes, and it can be used to determine the chemical composition of materials.

High-resolution scans were made of the O1s and V2p photoelectron peaks of both samples: on *a*- and *c*-plane Al₂O₃ substrates using a PHI Model 04-548 x-ray source with 15-255G electron analyzer with Al source twin-anode voltage of 15 kV and emission current of 11 mA under an operating pressure of 1×10^{-8} Torr in an attempt to determine the bonding states of the V and O. This bonding state is determined by comparing measurements of photoelectron binding energies in these samples with those found for V₂O₃ in the literature. It was found that both materials reasonably fit the reported binding energies for both V and O in V₂O₃. In the V₂O₃ on

a-plane Al_2O_3 , the $V2p_{3/2}$ peak was found to be at 515.6 eV [Fig. 5(a)], while in the V_2O_3 on *c*-plane Al_2O_3 , the $V2p_{3/2}$ peak was found to be at 516.1 eV [Fig. 5(b)]. Both of these values fall within the range of 516.8–513 eV found in literature for V_2O_3 .^{22,23} In addition, the O1s peaks showed very good agreement with literature for V_2O_3 after deconvolution was performed to separate the O peak associated with V_2O_3 and the O peak from adsorbed OH ions or H_2O . In the V_2O_3 on *a*-plane Al_2O_3 , the O1s peak was found to be at 531.1 eV [Fig. 5(a)], while in the V_2O_3 on *c*-plane Al_2O_3 , the O1s peak was found to be at 531.3 eV [Fig. 5(b)]. Both of these values are within the range of 530.3–530.5 eV found in literature, although, admittedly, the O1s peak for V_2O_5 is also within this range.^{23,24}

Electrical properties of the films were determined at room temperature (RT) using a four-point probe (Lucas Labs 302 resistivity stand) measurement with a Keithley 2400 digital SourceMeter in the sense mode, with probes

placed perpendicular to surface of the film. A current of 1.0 mA was injected through the two outer probes, and a voltage of 2.1 V was measured between the two inner probes. The RT resistivities for V_2O_3 films on *a*- and *c*-plane sapphire were 1.49×10^{-4} and $3.00 \times 10^{-5} \Omega m$, respectively (an error of ~3% in the resistivity measurements exists on the average). The measured resistivities indicated that both samples are metallic at RT as expected.

The bulk resistivity of V_2O_3 at RT is $\sim 1 \times 10^{-6} \Omega m$.¹⁴ A host of reasons may contribute to the degradation of the conductivity in oxides in thin film form, including crystallographic orientation (anisotropy), microstructural features such as grain boundaries, dislocations, and point defects, and internal stresses. An obvious factor is the presence of internal stresses in thin film as these directly modify the phase-transformation temperature. This is a phenomenon that can be described from basic thermodynamics and results in Clausius–Clapeyron type of relations. Furthermore, in thin films microstructural features develop primarily as to minimize the internal stresses. Therefore, the difference in resistivities of the films compared to bulk V_2O_3 as well as the difference in the resistivities of the films on *a*- and *c*-plane Al_2O_3 substrates can be attributed to internal stresses and microstructural variations that form to reduce the effect of the internal stresses.

Residual stresses arise primarily due to the lattice mismatch between the film and the substrate during the deposition and the thermal stresses that develop as the films are cooled down from the deposition temperature to RT due to the difference in the thermal expansion coefficients. We provide here a detailed discussion on the stress state of the *c*- and *a*-plane films to gain further insight on the difference between the bulk resistivity and the resistivities of the V_2O_3 films. To analyze the internal stress state of the films determined by the stress σ_i ($i = 1, 6$) and strain ϵ_i ($i = 1, 6$) tensors in the contracted notation, the following mechanical boundary conditions have to be taken into account: in-plane stresses $\sigma_1, \sigma_2 \neq 0$ and in-plane strains $\epsilon_1, \epsilon_2 \neq 0$, and shear stresses $\sigma_4 = \sigma_5 = \sigma_6 = 0$ and strains $\epsilon_4 = \epsilon_5 = \epsilon_6 = 0$. For a traction-free film surface, the out-of-plane strain $\sigma_3 = 0$ although $\epsilon_3 \neq 0$. For pseudomorphic V_2O_3 films on *a*-plane sapphire, the strain components are given by

$$\epsilon_1 = \frac{a_S - a_F}{a_S} \quad , \quad (1a)$$

$$\epsilon_2 = \frac{c_S - c_F}{c_S} \quad , \quad (1b)$$

$$\epsilon_3 = -\frac{C_{13}(\epsilon_1 + \epsilon_2)}{C_{33}} \quad , \quad (1c)$$

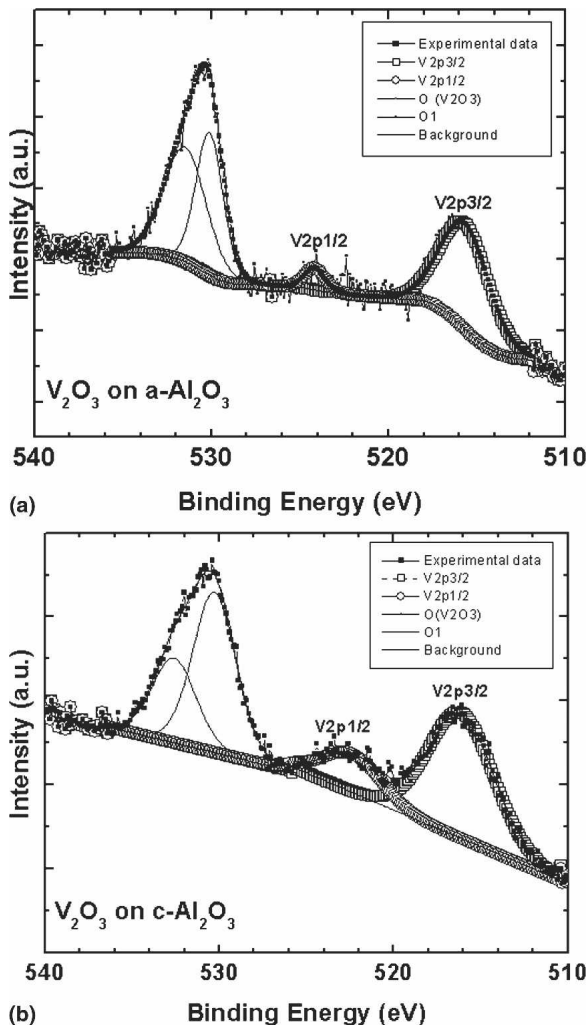


FIG. 5. XPS spectrum of V2p and O1s core levels of V_2O_3 films on (a) *a*-plane and (b) *c*-plane sapphire substrates.

resulting in an in-plane anisotropy, while on *c*-plane sapphire, the in-plane strain is isotropic, such that

$$\epsilon_1 = \epsilon_2 = \frac{a_S - a_F}{a_S} \quad , \quad (2a)$$

$$\epsilon_3 = -\frac{2C_{13}}{C_{33}} \epsilon_1 \quad , \quad (2b)$$

where a_S and c_S are the lattice parameters of the sapphire substrate, and a_F and c_F are the lattice parameters of bulk unconstrained V₂O₃ (Table I). C_{ij} are the elastic moduli³ of bulk V₂O₃ in the contracted notation. We can calculate the amount of out-of-plane strain, $\epsilon_3(\text{exp})$, in the films on *a*- and *c*-plane sapphire substrates from the measured values of the *d*-spacing of the films with respect to that of the bulk using the relation below:

$$\epsilon_3(\text{exp}) = \frac{d_B - d_F}{d_B} \quad , \quad (3)$$

where d_B and d_F are the *d*-spacings of the bulk and films, respectively (Table II).

Computations of the measured out-of-plane strain, $\epsilon_3(\text{exp})$ revealed that -0.4% and 1.1% strains (Table II) existed in the films on *c*- and *a*-plane Al₂O₃ substrates, respectively. These values differ from the calculated out-of-plane pseudomorphic lattice misfits, ϵ_3 (Table II). This suggests that the internal strains of the films depend strongly on the relaxation processes at the temperature of growth $T_G = 750^\circ\text{C}$ where interfacial dislocations may form to partially or completely relax in-plane strains due to lattice misfit.²⁰ The density (and thus the extent of relaxation) of the misfit dislocations is a function of the film thickness, although depending on the kinetics of the formation of these dislocations, their density might differ significantly from the equilibrium thermodynamic calculations.²⁵

Thermal strains, ϵ_i^{th} ($i = 1, 6$) will also develop as the films are cooled from T_G due to differences in thermal expansion coefficients (TECs) of the films,²⁶ α_F , and the substrates,²⁷ α_S . These strains usually cannot be relaxed by interfacial misfit dislocations mainly because of kinetic reasons as the film cools down.²⁸ The in-plane and out-of-plane components of the thermal strain on V₂O₃ film on *a*-plane sapphire substrate are given by

$$\epsilon_1^{\text{th}} = [\alpha_F(a) - \alpha_S(a)]\Delta T \quad , \quad (4a)$$

$$\epsilon_2^{\text{th}} = [\alpha_F(c) - \alpha_S(c)]\Delta T \quad , \quad (4b)$$

$$\epsilon_3^{\text{th}} = -\frac{C_{13}(\epsilon_1^{\text{th}} + \epsilon_2^{\text{th}})}{C_{33}} \quad , \quad (4c)$$

and are again anisotropic in the in-plane, while on *c*-plane sapphire substrate, we have

$$\epsilon_1^{\text{th}} = \epsilon_2^{\text{th}} = [\alpha_F(a) - \alpha_S(a)]\Delta T \quad , \quad (5a)$$

$$\epsilon_3^{\text{th}} = -\frac{2C_{13}}{C_{33}}\epsilon_1^{\text{th}} \quad . \quad (5b)$$

The resultant strain state in the film at ambient temperatures is therefore due to the interplay between the relaxation of the lattice misfit [Eqs. (1) and (2)] due to misfit dislocation formation at T_G and the thermal strains that develop during cooling from T_G [Eqs. (4) and (5)]. The residual strains in both samples are thus thermal strains that could not be relaxed by misfit dislocations.

It is obvious that the differences in the level of residual stresses, internal stress anisotropy and anisotropic strain relaxation, interfacial dislocation densities, as well as variations in the growth modes in the films on *a*- and *c*-plane sapphire will have a strong bearing on the electrical conductivity of the films. Films that grow in a layer-by-layer mode with lower levels of internal stresses and lower misfit dislocation densities, should have a better electrical conductivity. This might qualitatively explain why V₂O₃ films on *c*-plane sapphire have a lower resistivity compared to films grown on *a*-plane substrates. These results are consistent with observations reported in the literature. For example, earlier studies of the effects of pressure on single-crystal V₂O₃ has shown that negative pressure stabilizes the insulating phase while positive pressure stabilizes the metallic phase.²⁹ Similar effects have been found to occur in thin films depending on the type of substrates on which the film is grown. The compressive strain effect on V₂O₃ thin films (5–18 nm) by *c*-plane sapphire substrates tends to stabilize the metallic phase, i.e., suppression of the MIT with attendant increase in conductivity as the growth temperature decreases.¹⁵ On the other hand, tensile strain effect on V₂O₃ thin film by LiTaO₃ (001) substrate has been shown to favor the MIT.¹⁵ The internal stress state and the misfit dislocation spacing can be tuned systematically via changing the film thickness. Therefore, it becomes possible to investigate the role of the misfit strain and the interfacial defect structure on the electrical properties and the MIT characteristics of V₂O₃ films by simply varying the film thickness. These results will be presented in the future.

IV. CONCLUSION

In summary, epitaxial films of V₂O₃ are grown on *a*-plane Al₂O₃ substrates using PLD with a powder-pressed V₂O₃ target in an evacuated deposition chamber devoid of O₂ pressure (and the results are consistent with the epitaxy on the *c*-plane substrate as well). This approach seems very straightforward and simple, as no reduction process of V₂O₅ under controlled deposition atmosphere was involved. XRD patterns revealed the

crystalline orientation of the films on both substrates and its epitaxial nature was confirmed by XAFS. AFM images revealed that the films grew smoothly on the selected substrates with the films on *c*-plane sapphire having an almost 2D growth. XPS revealed that the stoichiometry of the film is well conserved in the vanadium oxide films. Electrical resistivity measurements confirmed that the films are metallic at room temperature as expected. Strain analysis indicated that the films relaxed much better on the *c*-plane sapphire substrate and accounted for the better quality of the film in terms of surface roughness and electrical conductivity.

ACKNOWLEDGMENTS

B. Allimi and S.P. Alpay gratefully acknowledge support by the United States Army Research Office (Grant W911NF-05-1-0528). We thank C. Xie, R. Nath, and R. Ristau for their help in the characterization of the samples and B.O. Wells for many useful discussions. The NSLS is supported by the Divisions of Materials and Chemical Sciences of the United States Department of Energy. We express our appreciation to the staff of the X-18 B line at the NSLS. T. Huang, D. Pease, and A. Frenkel acknowledge support by United States Department of Energy (Grant No. DE-FG02-05ER36184).

REFERENCES

1. M. Imada, A. Fujimori, and Y. Tokura: Metal-insulator transitions. *Rev. Mod. Phys.* **70**, 1039 (1998).
2. D.B. McWhan and J.P. Remeika: Metal-insulator transition in (V_{1-x}Cr_x)₂O₃. *Phys. Rev. B* **2**, 3734 (1970).
3. P.D. Dernier and M. Marezio: Crystal structure of the low-temperature antiferromagnetic phase of V₂O₃. *Phys. Rev. B* **2**, 3771 (1970).
4. I.S. Elfimov, T. Saha-Dasgupta, and M.A. Korotin: Role of *c*-axis pairs in V₂O₃ from the band-structure point of view. *Phys. Rev. B* **68**, 113105 (2003).
5. G. Kotliar: Driving the electron over the edge. *Science* **302**, 67 (2003).
6. J-H. Park, L.H. Tjeng, A. Tanaka, J.W. Allen, C.T. Chen, P. Metcalf, J.M. Honig, F.M.F. de Groot, and G.A. Sawatzky: Spin and orbital occupation and phase transitions in V₂O₃. *Phys. Rev. B* **61**, 11506 (2000).
7. M. Yethiraj: Pure and doped vanadium sesquioxide: A brief experimental review. *J. Solid State Chem.* **88**, 53 (1990).
8. P. Limelette, A. Georges, D. Jérôme, P. Wzietek, P. Metcalf, and J.M. Honig: Universality and critical behavior at the Mott transition. *Science* **302**, 89 (2003).
9. K.D. Rogers, J.A. Coath, and M.C. Lovell: Characterization of epitaxially grown films of vanadium oxides. *J. Appl. Phys.* **70**, 1412 (1991).
10. H. Schuler, S. Klimm, G. Weissmann, C. Renner, and S. Horn: Influence of strain on the electronic properties of epitaxial V₂O₃ thin films. *Thin Solid Films* **299**, 119 (1997).
11. J. Piao, S. Takahashi, and S. Kohiki: Preparation and characterization of V₂O₃ powder and film. *Jpn. J. Appl. Phys., Part 1* **37**, 6519 (1998).
12. I. Yamaguchi, T. Manabe, T. Kumagai, W. Kondo, and S. Mizuta: Preparation of epitaxial V₂O₃ films on C-, A- and R-planes of α-Al₂O₃ substrates by coating-pyrolysis process. *Thin Solid Films* **366**, 294 (2000).
13. Q. Luo, Q.L. Guo, and E.G. Wang: Thickness-dependent metal-insulator transition in V₂O₃ ultrathin films. *Appl. Phys. Lett.* **84**, 2337 (2004).
14. B. Sass, C. Tusche, W. Felsch, N. Quaas, A. Weismann, and M. Wenderoth: Structural and electronic properties of epitaxial V₂O₃ thin films. *J. Phys.: Condens. Matter* **16**, 77 (2004).
15. S. Yonezawa, Y. Muraoka, Y. Ueda, and Z. Hiroi: Epitaxial strain effects on the metal-insulator transition in V₂O₃ thin films. *Solid State Commun.* **129**, 245 (2004).
16. S. Autier-Laurent, B. Mercey, D. Chippaux, P. Limelette, and C. Simon: Strain-induced pressure effect in pulsed laser deposited thin films of the strongly correlated oxide V₂O₃. *Phys. Rev. B* **74**, 195109 (2006).
17. J. Piao, S. Takahashi, and S. Kohiki: Preparation of Cr-doped V₂O₃ films by sol-gel processing and their resistivity-temperature characteristics. *J. Ceram. Soc. Jpn.* **107**, 375 (1999).
18. C.N.R. Rao and B. Raveau: *Transition Metal Oxides: Structure, Properties and Synthesis of Ceramic Oxides*, 2nd ed. (Wiley-VCH, New York, 1998).
19. A.I. Frenkel, D.M. Pease, J.I. Budnick, P. Metcalf, E.A. Stern, P. Shanthakumar, and T. Huang: Strain-induced bond buckling and its role in insulating properties of Cr-doped V₂O₃. *Phys. Rev. Lett.* **97**, 195502 (2006).
20. J.W. Matthews and A.E. Blakeslee: Defects in epitaxial multilayers: I. Misfit dislocations. *J. Cryst. Growth* **27**, 118 (1974).
21. I.B. Misirlioglu, A.L. Vasiliev, M. Aindow, S.P. Alpay, and R. Ramesh: Threading dislocation generation in epitaxial (Ba,Sr)TiO₃ films grown on (001) LaAlO₃ by pulsed laser deposition. *Appl. Phys. Lett.* **84**, 1742 (2004).
22. N.K. Nag and F.E. Massoth: ESCA and gravimetric reduction studies on V/Al₂O₃ and V/SiO₂ catalysts. *J. Catal.* **124**, 127 (1990).
23. A.F. Werfel and A.O. Brummer: Corundum structure oxides studied by XPS. *Phys. Scr.* **28**, 92 (1983).
24. R.J. Colton, A.M. Guzman, and J.W. Rabalais: Electrochromism in some thin-film transition-metal oxides characterized by x-ray electron spectroscopy. *J. Appl. Phys.* **49**, 409 (1978).
25. S.P. Alpay, V. Nagarajan, L.A. Bendersky, M.D. Vaudin, S. Aggarwal, R. Ramesh, and A.L. Roytburd: Effect of the electrode layer on the polydomain structure of epitaxial PbZr_{0.2}Ti_{0.8}O₃ thin films. *J. Appl. Phys.* **85**, 3271 (1999).
26. L.J. Ekert and R.C. Bradt: Thermal expansion coefficient of corundum structure Ti₂O₃ and V₂O₃. *J. Appl. Phys.* **44**, 3470 (1973).
27. W.J. Campbell and C. Grain: Thermal expansion of alpha alumina. U.S. Bureau of Mines Technical Report No. BM-RI-5757 (Bureau of Mines, College Park, MD, 1960), p. 16.
28. I.B. Misirlioglu, S.P. Alpay, F. He, and B.O. Wells: Stress induced monoclinic phase in epitaxial BaTiO₃ on MgO. *J. Appl. Phys.* **99**, 104103 (2006).
29. D.B. McWhan, J.P. Remeika, T.M. Rice, W.F. Brinkman, J.P. Maita, and A. Menth: Electronic specific heat of metallic Ti-doped V₂O₃. *Phys. Rev. Lett.* **27**, 941 (1971).
30. A.I. Frenkel, E.A. Stern, and F.A. Chudnovsky: Metal-insulator transition and local structure of V₂O₃. *J. Phys. IV, Colloque C2* **7**, 1061 (1997).